JMC Publication
SINCE 1951

JOURNAL OF ADVANCED APPLIED SCIENTIFIC RESEARCH, Vol. 4, No. 3, 1-7, 2022
https://doi.org/10.46947/joaasr432022238

Green facile synthesis of Ag-doped ZnO nanoparticles from Gymnema sylvestre leaf extract and investigation of their Antibacterial activity

P. Vijaya Kumar[1], M. Karthikeyan[2]*,A. Jafar Ahamed [3],A. Ravikuma[4]B. Ragavi[2]

Abstract
The unique characteristics of the green synthesis pathway have opened the way for a new field of scientific investigation. Gymnema sylvestre (G. sylvestre) leaves extract was employed as a reducing and capping agent in the current investigation to produce pure zinc oxide (ZnO) (G1) and silver doped zinc oxide (Ag doped ZnO) (G2) nanoparticles (NPs). XRD, FESEM, EDAX, and FT-IR investigations stood used to study the structural characterization of G1 and G2 NPs. The UV–Vis and PL analyses were used to examine the optical characteristics. The results clearly reveal that the leaf extract is the best possible stabilizing agent for the manufacture of G1 and G2 NPs, and that the generated nanoparticles operate as potent microbial agents, inhibiting the growth of a variety of dangerous microbes. Due to their eco–friendly and non–toxic compatibility, the prepared G1 and G2 NPs can be employed for therapeutic and other purposes.

Keywords
Zinc Oxide, Nanoparticles, Gymnema sylvestre, characterization, antimicrobial activity.

[1] *Department of Chemistry, Jairams Arts and Science College, Affiliated to Bharathidasan University, Karur- 639 003, Tamil Nadu, India.*
[2] *Department of Chemistry, Periyar Maniammai Institute of Science and Technology, Vallam, Thanjavur- 613 403, Tamil Nadu, India.*
[3] *Post Graduate and Research Department of Chemistry, Jamal Mohamed College (Autonomous), Affiliated to Bharathidasan University, Tiruchirappalli - 620 020, Tamil Nadu, India.*
[4] *Department of Chemistry, SRM TRP Engineering College, Tiruchirappalli,Tamil Nadu – 621 105*
***Corresponding author**: karthichemist10@gmail.com

1. Introduction

Nanotechnology is a widely used and successful technology that is employed in a different fields, like biomaterials, nanomedicines, nanoelectronics, energy processing, and consumer goods. In a variety of industries, including electrical devices and biosensors, silver (Ag) and ZnO NPs with antibacterial properties have been discovered. [1,2]. Also, hybrid nanotechnologies have recently gotten a plenty of attention since they allow for new and improved functionality by altering the surface of each particle [3].

Pure ZnO nanostructures are prone to optical and structural flaws such as point defects, oxygen vacancies, and other flaws [4]. As a result, pure ZnO nanostructures are unsuitable for industrial use. To compensate for these flaws, ZnO nanostructures must be doped with noble metals. Platinum and gold-doped ZnO NPs have been shown in numerous studies [5] to have superior catalytic activity than pure ZnO. Platinum, like gold, is a very cost-effective material for industrial use. Due to the inexpensive cost of silver when compared to other metals, silver-based products are regarded as acceptable for industrial applications [6–8]. Consequently, in the modern world, most researchers are focusing on adding Ag NPs to ZnO to make the composite work better [9].

Furthermore, antibacterial activities of ZnO NPs have been demonstrated against oral microorganisms that cause tooth decay. Metal oxide NPs be present originate to be effective in bacterial control, for both gram-negative (G+) and gram-positive (G-) bacteria than bigger particles [10–12]. Synergistic antibacterial activity (ZnO/Ag) have been found to have a substantial impact against G+ and G- bacteria than their constituents [13]. When ZnO-Ag NPs are combined, bacterial activity and the formation of reactive oxygen species (ROS) are expected to rise. [14–15].

In this study, G. sylvestre leaf extract is used as a capping and reducing agent to manufacture of Ag2+ doped ZnO NPs. Investigations are performed on the structural, optical, and morphological characteristics of natural leaf extract and Ag2+ doped ZnO NPs, as well as their good applications in antibacterial activities.

Table 1. X-ray diffraction parameter values of the G1 and G2 samples

Samples	Lattice parameter values (nm)		Atomic packing factor (c/a)	Volume (V) (Å)^3	Cos ϕ	Position parameter	Bond Length (Zn-O) L (Å)	Average crystallite size D (nm)
	a	c						
G1	3.2557	5.2155	1.6019	47.876	0.9459	0.3798	1.5569	44
G2	2.9597	4.9645	1.6773	37.661	0.9477	0.3684	1.4801	32

2. Materials and methods

2.1 Synthesis of ZnO and Ag doped ZnO NPs

15 g of G. sylvestre leaves were cleaned many times with tap and twice distilled water to make ZnO. The leaves were then boiled for 1 hour at 80°C in a beaker with 150 mL of deionized water. The Whatman filter paper was used to filter the leaf extract. 150 mL of G. sylvestre leaf extract was dissolved in 0.1 M Zn (NO3)2. 6H2O ZnO NPs solution. The uniformly mixed nitrate solution was agitated continuously for 6 h at 80 oC. The result was a yellow precipitate formed and dried for 2 h at 120 °C. The ZnO (G1) produced was calcinated at 700 °C for 5 h before being stored in a sealed container. Additionally, Ag doped ZnO, 0.002 M AgNO3 was added to 0.098 M Zn(NO3)2.6H2O, which was then dissolved in 150 ml of G. sylvestre leaves extract. The aforementioned combination was then applied uniformly and continuously stirred at 80 0C for 6 h to obtain the final product. To obtain Ag doped ZnO NPs, it was dried for two hours at 120 0C. (G2). The product was calcined at 700 0C for 5h. Figure 1 shows the process flow for producing G1 and G2 NPs.

2.2 Techniques of characterization

The structural properties of synthesized G1 and G2 NPs were tested using X-ray powder diffraction (X'PERT PRO PAN analytical) and Fourier Transform Infrared Spectrometer (Perkin-Elmer). The Gemini 300 (Carlzeiss) FESEM was used to report the morphology and elemental analysis of the samples. Perkin-Elmer was used to measure the NPs' absorption spectrum (Lambda 35). The NPs' PL emission was examined using a Perkin Elmer LS45 spectrofluorometer.

The well diffusion technique was adopted to perform the antibacterial activities of G1 and G2 NPs for two bacterial species, namely G+ bacteria like Staphylococcus aureus and G- Bacteria like Klebsiella pneumoniae. The antibacterial activity was investigated with the help of the required number of NPs mixed in dimethyl sulphoxide at a concentration of 1.5 mg/ml. The zone of inhibition measures (mm) was assessed after 24 hours, and the sample had been incubated 24 h at 37 °C prior to this phase. As a positive control, the antibiotic Amoxicillin was utilized.

3. Results and Discussion

3.1 XRD Studies

The X-ray diffraction pattern for G1 and G2 NPs synthesized using G. sylvestre leaf extract are shown in Fig. 2a. The XRD peaks noted at (2) of 31.642, 34.409, 36.161, 47.444, 56.589, 62.845, 66.242, 67.872, 68.994 and 77.018 correspond to the (100), (002), (101), (102), (110), (103), (112), (201), (004) and (202) planes of the ZnO NPs and also showed the hexagonal wurtzite structure with the p63mc space group. The JCPDS data further supports this (Card no. 36-1451). For Ag2+ doped ZnO (G2) NPs, there isn't an impurity phase visible.

An enhanced representation of the XRD pattern between 35.6° and 36.6° is displayed in Fig. 2b to study the impact of Ag2+ doping on structure. It is important to note that the angle shift is somewhat higher than that of ZnO NPs, indicating that Ag2+ has been doped in ZnO in accordance with Vegard's law.

Zn2+ and Ag2+ have ionic radii of 0.74 and 1.26, respectively. The relation can be used to determine the lattice constants 'a' and 'c' of the wurtzite structure.

$$\frac{1}{d^2} = \frac{4}{3}\left(\left(\mu + hk + k^2\right)/a^2\right) + \frac{l^2}{c^2}$$

with the (100) plane's first order approximation (n = 1).

The relation a = /3 sin the lattice constant "a," and the relation c = / sin the lattice constant "c" for the plane (002). For ZnO NPs, the computed values of "a" and "c" are 3.2557 and 5.2155 respectively. When Ag2+ ions are substituted at ZnO lattice sites, the lattice constants "a" and "c" become less significant compared to the lattice constant of pure ZnO NPs, and their values are listed in Table 1. These result from the silver atoms shifting into a more equilibrated state after being trapped in non-equilibrium positions.

$$V = \frac{3a^2c}{2} = 0 \cdot 866a^2c$$

For G1 and G2 NPs, the unit cell volumes estimated using the aforementioned relation are determined to be 48.0354 and 47.9769 correspondingly. This demonstrates that all of these ions partially occupy tetrahedral Zn positions (Table 1). The differences in the values imply that while Ag2+ ions are present at the normal lattice site of ZnO, they also cause crystal defects near the dopants, which change the materials' stoichiometry. Utilizing relation, the bond length (L) of Zn-O is determined [16].

$$l = \sqrt{(a^2/3 + (1/2 - u)^2 XC^2)}$$

where "a" and "c" stand for lattice parameters and "u" for positional parameter, which represents the distance between each atom and the one after it along the "c" axis. The equation can be used to determine the parameter $u = a^2/(3c^2) + 0.25$

There is a strong correlation between c/a ratio and 'u'. Because of a distortion of tetrahedral angels caused by long-range polar contact, the c/a ratio increases as 'u' decreases, allowing those four tetrahedral distances to remain almost constant. In comparison to pure ZnO NPs, the c/a ratio of Ag2+ doped ZnO (G2) NPs decreased in our study (Table 2). For G1 and G2 NPs, the bond length of Zn-O is determined to be 1.5569 and 1.4801, respectively. The average crystallite size of the samples is estimated using Debye Scherrer's formula. Average crystallite size D= $(k\lambda/\beta cos\theta)$

In this formula D,λ,k and is the size in nanometers,the wavelength of ther maximum in radians.

The average particle sizes of the G1 and G2 NPs were found to be 44 nm and 32 nm, respectively. As opposed to G1 NPs, the G2 NPs have smaller particle sizes. Ag2+ ion

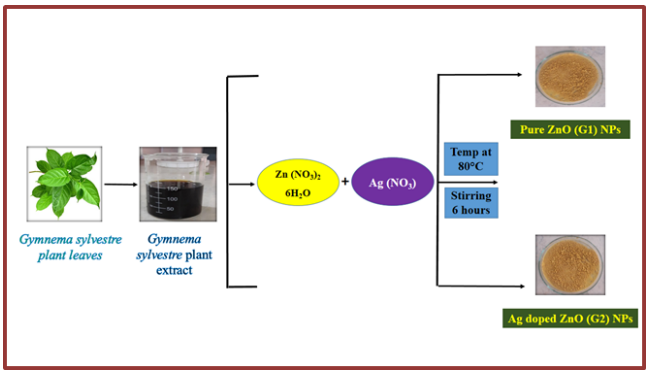

Figure 1. Synthesis of G1 and G2 NPs.

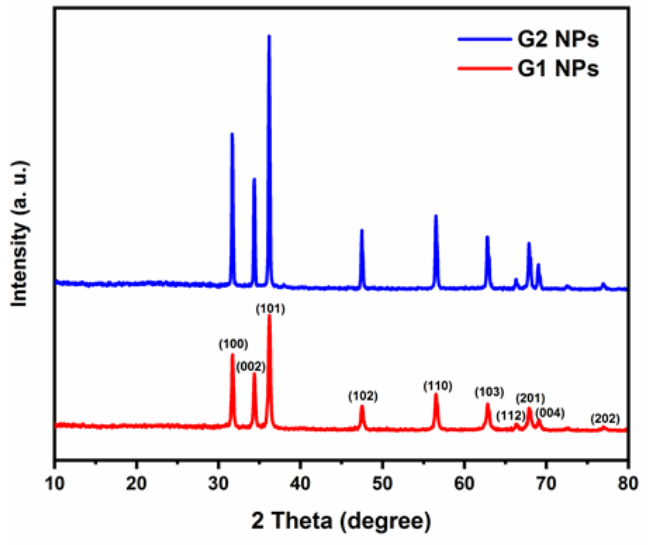

Figure 2. XRD patterns of G1 and G2 NPs

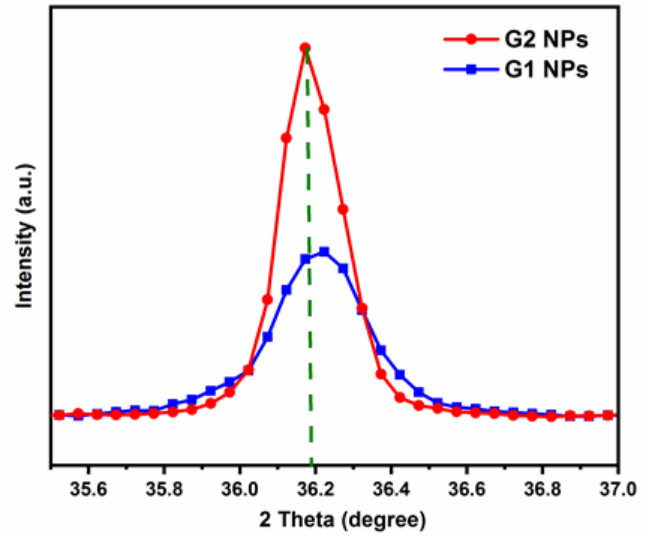

Figure 3. The zoomed version of the XRD pattern for G1 and G2 NPs

distortion of the host ZnO lattice, which lowers the nucleation and subsequent growth rate of the ZnO NPs, is the primary cause of the reduction in particle size.

3.2 FT-IR analysis

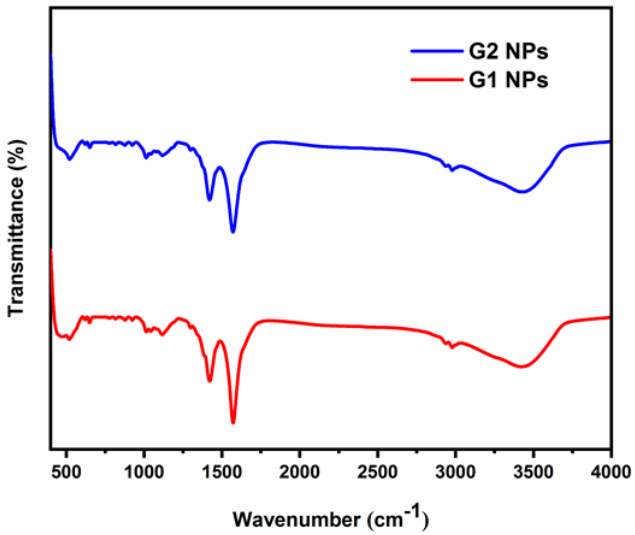

Figure 4. FT-IR spectra of G1 and G2 NPs

The FT-IR spectrum of the G1 and G2 NPs is depicted in Figure 3. The O-H band's vibrational stretching mode is reflected by a peak between the range of 3020–3650 cm-1 [17]. The peak at 467 cm-1 was discovered to be connected to Zn-O stretching in G1 NPs, while the Zn-O stretching vibration was determined to be 521 cm-1 in G2 NPs. For both G1 and G2 NPs, asymmetric C-O stretching bands can be identified at 1117 cm-1, whereas asymmetric C-H stretching bands can be discovered at 2937 cm-1.

3.3 FE-SEM and EDAX analysis

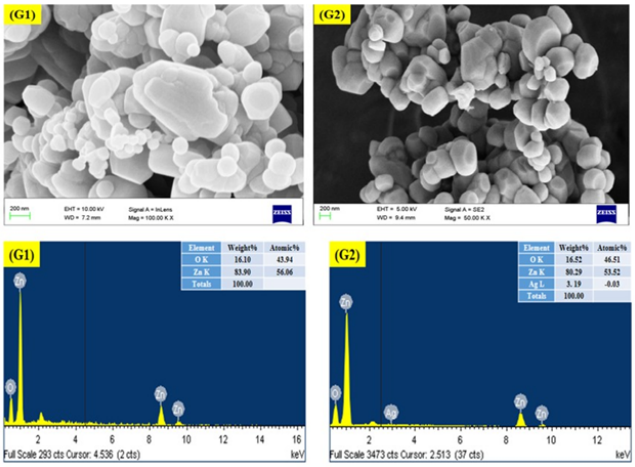

Figure 5. Surface morphology and elemental analysis of G1 and G2 NPs using G. sylvestre leaf extract

Fig.4 shows the morphology of G1 and G2 NPs produced

with G. sylvestre leaf extract. In Fig.4, the spherical and hexagonal nanostructures of the G1 and G2 NPs were clearly visible. For G1 and G2 NPs, the particle size was calculated to be 42 nm and 38 nm, respectively. The formation of ZnO NPs in G2 NPs is slowed down by the Ag2+ ions, which makes the nanoparticles thinner. Elemental analysis G1 and G2 NPs prepared by G. sylvestre leaf extract was performed by EDAX spectra are shown in Fig.4. It shows that the produced nanoparticles in both samples contain Zn, Ag, and O. (G1 and G2). The degree of strength of the atomic percentages of the elements in these samples varies slightly. This demonstrates that in the green synthesis process, leaf extracts (alkaloids, tannins, saponins, phenols, glycosides, and flavonoids) work as capping and reducing agents.

3.4 UV–Vis absorption spectroscopy

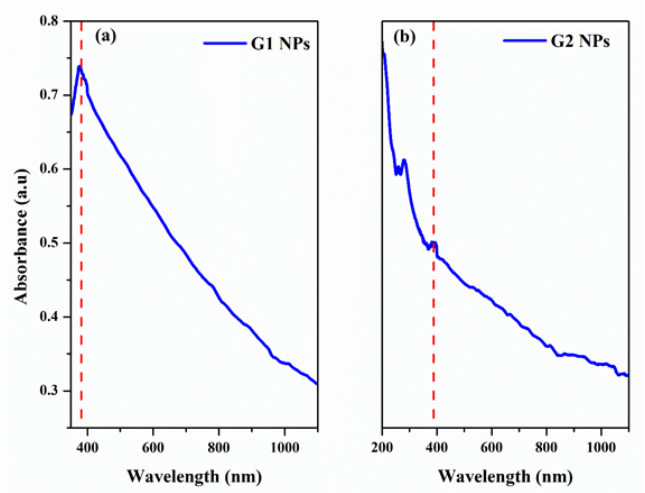

Figure 6. UV-vis spectrum of a) G1 and b) G2 NPs

Fig. 5 depicts UV–visible optical absorption spectra in the wavelength scale of 350–800 nm. The G1 and G2 NPs were disseminated equally in distilled water before being ultrasonified for 15–20 minutes and UV–Vis spectra collected. G1 NPs' absorption peak was seen at wavelengths of 374 and 397 nm, respectively, as a result of the photoexcitation of electrons in the valence band and conduction band. [18]

3.5 Photoluminescence (PL) studies

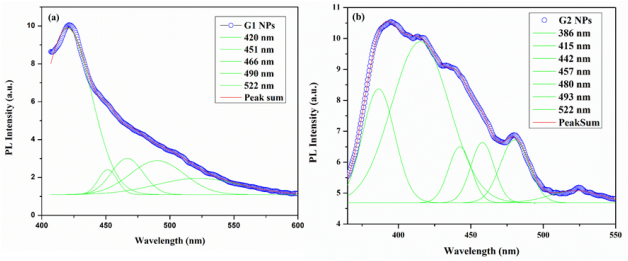

Figure 7. (a b) PL emission spectra of G1 and G2 NPs

Fig. 6 (a-b) displays the PL spectra of synthesised G1 and G2 NPs recorded at the excited wavelength of 385 nm. For G1 and G2 NPs, PL emissions are seen at wavelengths ranging from very short (400 nm) to extremely long (600 nm). The recorded spectra for both ZnO NPs were fitted using a Gaussian function with five peaks. The solid lines show a linear combination of five Gaussian peaks, with the minimum and maximum wavelengths being 420 nm and 522 nm, respectively. The emission spectra of the G1 NPs are having five peaks at (420, 451, 466, 490 and 522 nm) and G2 NPs having seven peaks at (386, 415, 442, 457, 480, 493 and 522nm) respectively. These wavelengths correspond to the emission of violet, blue, blue-green, and green light, respectively. The near-band emission (NBE) of ZnO NPs, which corresponds to the UV emission peaks of lowest wavelength, is observed at 386 nm. An electron transfer from a shallow donor level of the natural zinc interstitials to the top level of the valence band is attributed to the three violet emissions centred at 415, 420, and 442 nm [19]. The transition between interstitial oxygen and oxygen vacancies is responsible for the blue-green fluorescence shown at 451, 457, 466, 480, and 493 nm [20]. Finally green emissions at 522 nm are due to singly ionized oxygen vacancies [21, 22].

Table 2. G1 and G2 NPs exhibit antimicrobial properties against human diseases

Samples	S.aureus	K. pneumoniae
Std	1	0.8
G1 NPs	1.5	1.2
G2 NPs	1.8	1.6

3.6 Antimicrobial activity

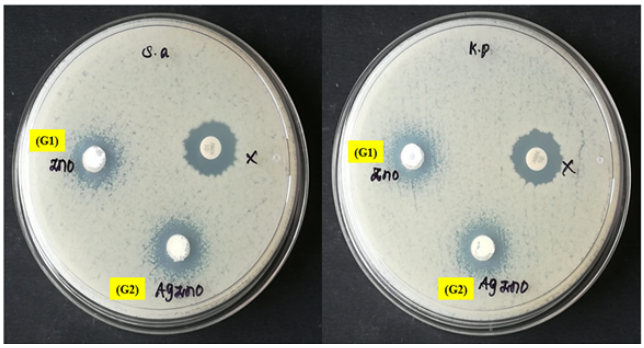

Figure 8. Zone of inhibition of G1 and G2 NPs against S. aureus and K. pneumoniae

At a concentration of 1.5 mg/ml, the antibacterial activity of green-generated G1 and G2 NPs is shown in Fig. 7. According to this study, G2 NPs have a stronger antibacterial impact than G1 NPs. The results of antibacterial activity are given in Table 2. Based on the findings, the zones were raised in proportion to the concentration of Ag2+ ion dopant against the bacteria studied. Because of differences in cell wall structure and composition, the G+ bacteria have a larger inhibitory zone than the G-bacteria. The particle size of the G2 NPs was

Table 3. Comparison of antimicrobial values of current study and different metals doped ZnO NPs on various bacterial strains

S.No	Concentration	Materials	Size	Bacteria
Present study				
1.	1.5mg/ml	0.098 % of ZnO	44 nm	Staphylococcus aureus
2		0.002 % of Ag in ZnO	32 nm	
Previous studies				Klebsiella pneumoniae
1	20 (g/mL)	(1, 3, and 5 wt % of Cu doped ZnO [25]	30 nm	Escherichia coli, Staphylococcus aureus
2	1 (mg/ml)	0.01 % of La3+ doped ZnO [26]	38 nm	Staphylococcus aureus Streptococcus pneumoniae
3	1 mg/ml, 3 mg/ml and 5 mg/ml	0.005 % of Mg in ZnO [27]	42 nm	Staphylococcus aureus, Escherichia coli
4	25 (g/mL)	(1, 3, and 5 wt % of Ag doped ZnO [28]	48 nm	Staphylococcus aureus
5	1 (mg/ml)	0.05 % of Zr doped ZnO [29]	37 nm	Bacillus subtilis, Klebsiella pneumoniae
6	10 (mg/ml)	0.03, 0.05, 0.07 M % of La doped in ZnO [30]	13, 11 & 10 nm	Staphylococcus aureus, Proteus mirabilis, Salmonella typhii and Bacillus subtilis

32 nm, which is related to higher antibacterial activity. [23] When NPs with uneven surfaces as well as the rough edges are created, antibacterial studies demonstrate that they can link to the bacteria's wall and harm the cell membrane.

The mechanism of the G1 and G2 NPs that exhibited the antibacterial activity is shown in Fig.8. As seen in the FESEM image, G1 and G2 NPs have a variety of morphologies, including spherical and hexagonal structures. The Ag doped ZnO NPs (G2) have uneven ridges on their outer surface, which led to antibacterial activity while other NPs' flat surfaces did not. This shows that antibacterial activity is significantly more effective on unevenly ridged surfaces [23]. Increased Ag doping in ZnO NPs creates more defects, according to photoluminescence studies (PL). The PL study of Ag2+ doped ZnO NPs (G2) demonstrates that green emission rises when oxygen vacancies form in response to the dopant [24]. Antibacterial

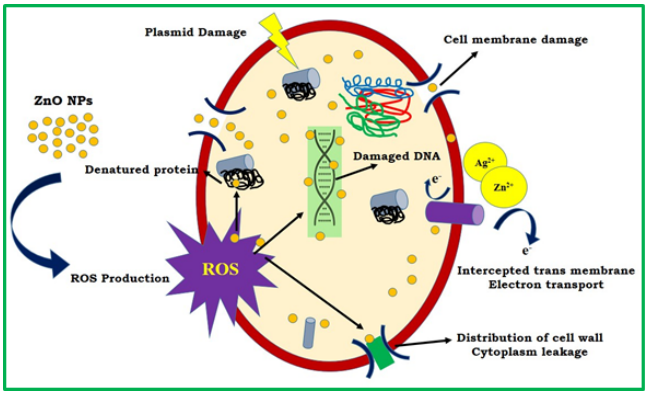

Figure 9. Antibacterial mechanism of G1 G2 NPs against bacterial pathogens

experiments show that G2 NPs are more effective than G1 NPs.

The current experiment demonstrated that pure and Ag2+ doped ZnO NPs exhibit minimal antibacterial activity based on the comparative statement. It's worth mentioning that all of the samples were effective against G+ and G-bacteria. Table 3 compares the concentrations of various metals doped ZnO NPs necessary to prevent the growth of human diseases to those reported in the literature [25-30].

4. Conclusion

Using G. sylvestre leave extract as a starting point, the G1 and G2 NPs were successfully synthesized. The hexagonal wurtzite structure of the G1 and G2 NPs generated, with average particle sizes of 42 and 37 nm, was confirmed by XRD examination. G2 NPs have a smaller size when compared to G1 NPs. External contaminants, such as Ag2+ ions, cause deformation in the host ZnO lattice, resulting in a reduction in size. The elemental composition was calculated using the EDAX spectra. The UV-Vis investigations backed up the optical absorption findings. The PL studies revealed the doping materials change the band emission, which is related to zinc/oxygen vacancies and surface defects. The G2 NPs outperformed the others in antibacterial experiments on a variety of bacterial species. It was discovered that the antibacterial effects of ZnO NPs are due to a combination of reactive oxygen species and Zn2+ release. In the XRD device of Ag2+ doped ZnO NPs, no peak (impurity phase) that looked like Ag2+ was seen. This means that the impact was not caused by the release of Ag2+.

References

[1] Zhong C.J, Mave M.M. (2001) Core Shell assembled nanoparticles as catalysts. Adv. Mater., 13, 1507–1511.

[2] Alammar T, Mudring A.V. (2009) facile preparation of Ag/ZnO nanoparticles via photoreduction. J. Mater. Sci., 44, 3218–3222. 10.1007/s10853-009-3429-4

[3] Aguirre M.E, Rodriguez H.B, San Roman E, Feldhoff A, Grela M.A. (2011) Ag@ ZnO core-shell nanoparticles formed by the timely reduction of Ag+ ions and zinc acetate hydrolysis in N, N-dimethyl formamide: mechanism of growth and photocatalytic properties. J. Phys. Chem. C., 115, 24967–24974. https://doi.org/10.1021/jp209117s

[4] Ahmad M, Zhao J, Iqbal J, Miao W, Xie L, Mo R, Zhu J. (2009) Conductivity enhancement by slight indium doping in ZnO nanowires for optoelectronic applications. J. Phys. D Appl. Phys., 42, 165406. Doi : "10.1088/0022-3727/42/16/165406",

[5] Wang H, Wingett D, Engelhard M.H. (2009) Fluorescent dye encapsulated ZnO particles with cell-specific toxicity for potential use in biomedical applications. J. Mater. Sci. Mater. Med., 20, 11–22. DOI: 10.1007/s10856-008-3541-z

[6] Vidhya K, Saravanan M, Devarajan V.P, Subanya S, Bhoopathi G. (2015) Structural and optical characterization of pure and starch capped ZnO quantum dots and their photocatalytic activity. Appl. Nanosci., 5, 235–243. https://doi.org/10.1007/s13204-014-0312-7

[7] Yang S, Wang J, Li X, Zhai H, Han D, Wei B, Wang D, Yang J. (2014) One-step synthesis of birdcage-like ZnO and other controlled morphologies: structural, growth mechanism and photocatalytic properties. Appl. Surf. Sci., 319, 211–215. https://doi.org/10.1016/j.apsusc.2014.07.165

[8] Wu X, Wen L, Lv K, Deng K, Tang D, Ye H, Du D, Liu S, Li M. (2015) Fabrication of ZnO/graphene flake-like photocatalyst with enhanced photoreactivity. Appl. Surf. Sci., 358, 130–136. https://doi.org/10.1016/j.apsusc.2015.08.061

[9] Dias H.B, Bernardi M.I.B, Marangoni V.S, Bornardi A.C.A, Rastelli A.N.S, Hernandes A.C. (2019) Synthesis, characterization and application of Ag-doped ZnO nanoparticles in a composite resin. Matar. Sci. Engg. C., 96, 391–401. DOI: 10.1016/j.msec.2018.10.063

[10] Fang M, Chen J.H, Xu X.L, Yang P.H, Hildebrand H.F. (2006) Antibacterial activities of inorganic agents on six bacteria associated with oral infections by two susceptibility tests. Int. J. Antimicrob. Agents., 27, 513–517. DOI: 10.1016/j.ijantimicag.2006.01.008

[11] Adams L.K., Lyon D.Y., McIntosh A., Alvarez P.J.J. (2006) Comparative toxicity of nanoscale TiO2, SiO2 and ZnO water suspensions. Water Sci. Technol., 327–334. DOI: 10.2166/wst.2006.891

[12] Allaker R.P. The use of nanoparticles to control oral biofilm formation. (2010) J. Dent. Res., 89 1175–1186. DOI: 10.1177/0022034510377794

[13] Zhang Y, Gao X, Zhi L, Liu X, Jiang W, Sun Y, Yang J. (2014) the synergetic antibacterial activity of Ag islands on ZnO (Ag/ZnO) heterostructure nanoparticles and its mode of action. J. Inorg. Biochem., 130, 74–83. DOI: 10.1016/j.jinorgbio.2013.10.004

[14] Ghosh S, Goudar V.S, Padmalekha K.G, Bhat S.V, Indi S.S, Vasan H.N. (2012) ZnO/Ag nanohybrid: synthesis, characterization, synergistic antibacterial activity and its mechanism. RSC Adv., 2, 930. https://doi.org/10.1039/C1RA00815C

[15] Jim´enez A.B.P, Aguilar C.A.H, Ramos J.M.V, Thangarasu P. (2015) Synergistic antibacterial activity of nanohybrid materials ZnO-Ag and ZnO-Au: synthesis, characterization, and comparative analysis of undoped and doped ZnO nanoparticles. Aust. J. Chem., 68 (2015) 288–297. DOI: 10.1071/CH14123

[16] Karthikeyan B, Pandiyarajarn T, Mangaiyarkarasi K. (2011). Optical properties of sol–gel synthesized calcium doped ZnO nanostructures. Spectro- chim. Acta Part A., 82(1), 97–101. https://doi.org/10.1016/j.saa.2011.07.005

[17] Zandi, S., Kameli, P., Salamati, H., Ahmad, H., Hakimi, M. (2011). Microstructure and optical properties of ZnO nanoparticles prepared by a simple method. Physica B., 406, 3215- 3218. 10.1016/j.physb.2011.05.026

[18] Liu, M., Kitai, A. H., Mascher, P. (1992). Point defects and luminescence centres in zinc oxide and zinc oxide doped with manganese. J. Lumin., 54(1), 35-42. https://doi.org/10.1016/0022-2313(92)90047-D

[19] Fan, X. M., Lian, J. S., Zhao, L., Liu, Y. (2005). Single violet luminescence emitted from ZnO films obtained by oxidation of Zn film on quartz glass. Appl. Sur. Sci., 252, 420- 424. 10.1016/j.apsusc.2005.01.018

[20] Varghese, N., Panchakarla, L. S., Hanapi, M., Govindaraj, A., Rao, C. N. R. (2007). Solvothermal synthesis of nanorods of ZnO, N-doped ZnO and CdO. Mater. Res. Bull., 42, 2117- 2124. 10.1016/j.materresbull.2007.01.017

[21] Kumar, N., Dorfman, A., Hahm, J. (2005). Fabrication of optically enhanced ZnO nanorods and microrods using novel biocatalysts. J. Nanosci. Nanotech., 5, 1915-1918. https://doi.org/10.1166/jnn.2005.422

[22] Bagnall, D. M., Chen, X. F., Shen, M. Y., Zhu, Z., Goto, T., Yao, T. (1998). Room temperature excitonic stimulated emission from zinc oxide epilayers grown by plasma-assisted MBE. J. Cryst. Growth., 184, 605-609. DOI: 10.1016/S0022-0248(98)80127-9

[23] Karthikeyan M, Jafar Ahamed A, Karthikeyan C, Vijaya Kumar P. (2019). Enhancement of antibacterial and anticancer properties of pure and REM doped ZnO nanoparticles synthesized using Gymnema sylvestre leaves extract. SN Applied Sciences., 1, 355. https://doi.org/10.1007/s42452-019-0375-x

[24] Vijayaprasath G, Murugana R, Palanisamy S, Prabhu N.M, Mahalingam T, Hayakawa Y, Ravi G. (2016) Role of nickel doping on structural, optical, magnetic properties and antibacterial activity of ZnO nanoparticles. Materials Research Bulletin., 76, 48-61. https://doi.org/10.1016/j.materresbull.2015.11.053

[25] Raju P, Deivatamil D, Martin Mark J, Joseph Prince J. (2022) Antibacterial and catalytic activity of Cu doped ZnO nanoparticles: structural, optical, and morphological study. J Iran Chem Soc., 19, 861–872 (2022). https://doi.org/10.1007/s13738-021-02352-3

[26] Karthikeyan M, Jafar Ahamed A., Vijayakumar P, Karthikeyan C (2018) Green synthesis of pure ZnO and La doped ZnO nanoparticles and their structural, optical and antibacterial studies. Eur J Biomed Pharm Res 5 (2): 736-741.

[27] Jafar Ahamed A., Vijayakumar P, Karthikeyan M, (2016) Synthesis, Structural and Antibacterial Properties of Mg Doped ZnO Nanoparticles. J. Environ. Nanotechnol 5(2): 11-16.

https://doi.org/10.13074/jent.2016.06.162189

[28] Vikal S, Gautam Y K, Ambedkar A K, Gautam D, Singh J, Pratap D, Kumar A, Kumar S, Gupta M, and Singh B P, (2022) Structural, optical and antimicrobial properties

of pure and Ag-doped ZnO nanostructures. J. Semicond. 43(3): 1-10.

https://doi.org/10.1088/1674-4926/43/3/032802

[29] Indrajith Naik E. Bhojya Naik H.S, Viswanath R, Kirthan B.R, Prabhakara M.C (2020) Effect of zirconium doping on the structural, optical, electrochemical and antibacterial properties of ZnO nanoparticles prepared by sol-gel method. Chem. Data Collect 29: 100505. https://doi.org/10.1016/j.cdc.2020.100505

[30] Manikandan A, Manikandan E, Meenatchi B, Vadivel S, Jaganathan S.K, Ladchumananandasivam R, M. Henini, M. Maaza, Jagathrakshakan Sundeep Aanand (2017) Rare earth element (REE) lanthanum doped zinc oxide (La: ZnO) nanomaterials: Synthesis structural optical and antibacterial studies. J. Alloys Compd.723 (5): 1155-1161. https://doi.org/10.1016/j.jallcom.2017.06.336